

# Two-stage Optimal Dispatching of AC/DC Hybrid Active Distribution Systems Considering Network Flexibility

Yi Su, *Student Member, IEEE*, and Jiashen Teh, *Senior Member, IEEE*

**Abstract**—The increasing flexibility of active distribution systems (ADSs) coupled with the high penetration of renewable distributed generators (RDGs) leads to the increase of the complexity. It is of practical significance to achieve the largest amount of RDG penetration in ADSs and maintain the optimal operation. This study establishes an alternating current (AC)/direct current (DC) hybrid ADS model that considers the dynamic thermal rating, soft open point, and distribution network reconfiguration (DNR). Moreover, it transforms the optimal dispatching into a second-order cone programming problem. Considering the different control time scales of dispatchable resources, the following two-stage dispatching framework is proposed. ① The day-ahead dispatch uses hourly input data with the goal of minimizing the grid loss and RDG dropout. It obtains the optimal 24-hour schedule to determine the dispatching plans for DNR and the energy storage system. ② The intraday dispatch uses 15 min of input data for 1-hour rolling-plan dispatch but only executes the first 15 min of dispatching. To eliminate error between the actual operation and dispatching plan, the first 15 min is divided into three 5-min step-by-step executions. The goal of each step is to trace the tie-line power of the intraday rolling-plan dispatch to the greatest extent at the minimum cost. The measured data are used as feedback input for the rolling-plan dispatch after each step is executed. A case study shows that the comprehensive cooperative ADS model can release the line capacity, reduce losses, and improve the penetration rate of RDGs. Further, the two-stage dispatching framework can handle source-load fluctuations and enhance system stability.

**Index Terms**—Two-stage dispatching, network flexibility, renewable distributed generator, second-order cone programming (SOCP), alternating current (AC)/direct current (DC) hybrid active distribution system.

Manuscript received: July 18, 2022; revised: September 25, 2022; accepted: November 12, 2022. Date of CrossCheck: November 12, 2022. Date of online publication: November 28, 2022.

This work was supported by Universiti Sains Malaysia through Research University Team (RUTeam) Grant Scheme (No. 1001/PELECT/8580011).

This article is distributed under the terms of the Creative Commons Attribution 4.0 International License (<http://creativecommons.org/licenses/by/4.0/>).

Y. Su and J. Teh (corresponding author) are with the School of Electrical and Electronic Engineering, Universiti Sains Malaysia (USM), 14300 Nibong Tebal, Penang, Malaysia (e-mail: suy0328@student.usm.my; jiashenteh@usm.my).

DOI: 10.35833/MPCE.2022.000424

## NOMENCLATURE

### A. Indexes

$a, j$	Indexes of nodes connected to the $i^{\text{th}}$ node as the end/start node in alternating current (AC) grid
$b, m$	Indexes of nodes connected to the $n^{\text{th}}$ node as the end/start node in direct current (DC) grid
$i$	Index of nodes in AC grid
$l$	Index of lines in AC and DC grids
$n$	Index of nodes in DC grid
$S$	Index of nodes in AC and DC grids

### B. Sets

$\varphi_i^{AC}, \Phi_i^{AC}$	Sets of branches with the $i^{\text{th}}$ node as the start/end node in the AC grid
$\varphi_n^{DC}, \Phi_n^{DC}$	Sets of branches with the $n^{\text{th}}$ node as the start/end node in the DC grid
$\varpi^{AC}, \varpi^{DC}$	Sets of nodes in AC and DC grids
$D$	Set of dividing points
$X$	Decision variables
$\Delta X$	Differences of decision variables between rolling-plan dispatch and real-time feedback dispatch

$Y, Y_{t+\Delta t}^{ref}$	Apparent power of tie-line of real-time feedback dispatch and rolling-plan dispatch
---------------------------	---

### C. Variables

$d_{k-1}, d_k$	Start and end dividing points of the $k^{\text{th}}$ segment
$D(d_k)$	Similar diameter
$E(24, k)$	Day-ahead dispatch divided into $k$ segments
$E_{s,t}^{in}, E_{s,t}^{out}$	Binary variables associated with ESS charging and discharging at node $s$ during period $t$
$\tilde{I}_{j,i,t}$	Square of current magnitude through branch ( $j, i$ ) during period $t$
$\tilde{I}_{i,t}^{VSC}$	Square of current magnitude through inside of VSC at node $i$ during period $t$
$I_{DTR}$	Actual line current rating calculated by dynamic thermal rating (DTR)

$k$	Times of distribution network reconfiguration (DNR) in the day-ahead dispatch
$K_{ij,t}, K_{ji,t}$	Binary variables that indicate the power direction through branch $(i,j)$ during period $t$
$L_{\zeta, \zeta+1}$	Equivalent load demand of active distribution system (ADS) in hour $[\zeta, \zeta+1]$
$\bar{L}_{d_{k-1}, d_k}$	Equivalent load average value in segment $[d_{k-1}, d_k]$
$P_{ji,t}, Q_{ji,t}$	Active and reactive power through branch $(j,i)$ during period $t$
$P_{i,t}^{InAC}, Q_{i,t}^{InAC}$	Active and reactive power injections at node $i$ during period $t$
$P_{n,t}^{InDC}$	Active power injection at node $n$ during period $t$
$P_{i,t}^{sub}, Q_{i,t}^{sub}, P_{i,t}^{RDG}, Q_{i,t}^{RDG}$	Active and reactive power injections at node $i$ by substation and renewable distributed generators (RDGs) during period $t$
$P_{n,t}^{RDG}$	Active power injection at node $n$ by RDGs during period $t$
$P_{i,t}^{Load}, Q_{i,t}^{Load}, P_{i,t}^{VSC}, Q_{i,t}^{VSC}, P_{i,t}^{SOP}, Q_{i,t}^{SOP}$	Active and reactive power outflowing from node $i$ to load, voltage source converter (VSC), and soft open point (SOP) during period $t$
$P_{n,t}^{Load}$	Active power outflowing from node $n$ to load during period $t$
$P_{n,t}^{VSC}$	Active power injection at node $i$ by the AC grid through VSC
$P_{s,t}^{ESSout}, P_{n,t}^{ESSout}, P_{i,t}^{ESSout}$	Active power injections from energy storage systems (ESSs) at node $s, n, i$ during period $t$
$P_{s,t}^{ESSin}, P_{n,t}^{ESSin}, P_{i,t}^{ESSin}$	Active power outflowing to ESSs at node $s, n, i$ during period $t$
$P_{RDG,t}^{cut}$	Dropout of RDG during period $t$
$Q_{i,t}^{SVG}$	Reactive power injection by static var generator (SVG) at node $i$ during period $t$
$Q_{i,t}^{VSC}$	Reactive power flowing out from ideal VSC
$Q_c, Q_r, Q_s$	Convection heat loss parameter, radiated heat loss parameter, and total solar and sky radiated heat parameter
$R(T_c)$	AC resistance of conductor at temperature $T_c$
$T_a, T_c, V_w, \theta_w$	Micrometeorological variables of conductor temperature, ambient temperature, wind speed, and wind angle
$U_{i,t}$	Voltage of the $i^{\text{th}}$ node during period $t$
$U_{n,t}$	Voltage of the $n^{\text{th}}$ node during period $t$
$\tilde{U}_{i,t}$	Square of voltage magnitude at node $i$ during period $t$
$U$	Voltage of conductor
$Z_{ij,t}$	Binary variable associated with branch $(i,j)$ on/off during period $t$
$W_{s,t}^{ESS}$	Actual capacity of ESS at node $s$ during period $t$

#### D. Parameters

$\alpha, \beta$	Charging and discharging efficiencies of ESS
$\tan \theta_{RDG}$	Power factor of RDG
$\tau$	Constant used to control the switching between economic and safety dispatch
$\Delta t$	Charging and discharging unit time interval of ESS
$\Delta t_a, \Delta t_{ip}, \Delta t_{ir}$	Time slots of day-ahead dispatch, rolling-plan dispatch, and real-time feedback dispatch
$C_b, C_{RDG}$	Costs of grid loss and RDG dropout
$P_{i,t}^{RDG,f}$	Forecasted active power generated by RDGs at node $i$ during period $t$
$P_{max}^{ESS}$	The maximum charging and discharging rates of ESS
$P_{max}^{VSC}, P_{min}^{VSC}$	The maximum and minimum active power of VSC
$Q_{max}^{SVC}, Q_{min}^{SVC}$	The maximum and minimum values of static var compensator (SVC)
$Q_{max}^{VSC}, Q_{min}^{VSC}$	The maximum and minimum reactive power of VSC
$Q_{max}^{SOP}, Q_{min}^{SOP}$	The maximum and minimum reactive power of SOP
$R_{ji}, X_{ji}$	Resistance and reactance of branch $(j,i)$
$R_{in}, X_{in}$	Equivalent resistance and reactance of VSC
$S_l, S_{l,max}$	Actual and maximum capacity ratings of line
$S_{max}^{VSC}, S_{max}^{SOP}$	The maximum capacities of VSC and SOP
$U_{max}^{AC}, U_{min}^{AC}$	The maximum and minimum voltages of nodes in AC grid
$U_{max}^{DC}, U_{min}^{DC}$	The maximum and minimum voltages of nodes in DC grid
$W_{max}^{ESS}$	The maximum capacity of ESS

## I. INTRODUCTION

WITH the establishment of the goals of “carbon emission peak and carbon neutrality goals”, a large number of flexible resources, such as renewable distributed generators (RDGs), energy storage systems (ESSs), and microgrids, have been connected to distribution systems, thus making such systems more flexible but uncertain with regard to the source, network, and load [1]. Traditional control methods for distribution networks primarily adjust the operating state with power generation control, and use decentralized control and local balancing strategies [2] to regulate the voltage. However, these methods cannot realize continuous and rapid real-time adjustment [3]. Thus, the power grid lacks the ability of flexible adjustment and they are difficult to apply to alternating current (AC)/direct current (DC) hybrid active distribution systems (ADSs). A more serious issue is that the coupling between flexible resources amplifies fluctuations [4] and affects the safe operation of a distribution system. In addition, RDGs such as photovoltaics (PVs)

and wind turbines (WTs) are intermittent and significantly fluctuate, thus easily affecting the quality of power supplied to a distribution system [5]. Accordingly, numerous scholars have proposed ADSs, which use flexible control strategies that are suitable for accessing RDGs with high penetration rates [6].

Scholars have conducted numerous studies on the uncertainties of ADSs by utilizing stochastic programming, robust optimization, and interval notation. Stochastic programming generally assumes that random variables obey a given probability distribution (for example, assuming that the WT and PV forecasting errors obey a normal distribution [7], [8]) to model the uncertainty factor. However, this method is limited by the accuracy of the description of the uncertainty. Therefore, scholars have proposed a data-driven random variable model. References [9], [10] used historical data and different deep learning models to improve the accuracy of the WT and load predictions, respectively, in the short term. Unlike stochastic programming, robust optimization does not require setting a probability distribution for the uncertainty but directly determines the worst scenario in the uncertainty set. References [11]-[13] constructed a polyhedral uncertainty set for the output of WTs, which was used for the scheduling and planning of power systems [11]-[13]. Nevertheless, the results of robust optimization are conservative [14]. Some researchers have proposed the interval notation to expand the scheduling space. In particular, [15] introduced an interval probability to the concept of prediction for PVs instead of using traditional point forecasters to provide further information. The aforementioned methods focus on improving the prediction accuracy to reduce the uncertainty in the RDG output but ignore the complementarity of resources in the ADS. In response, some researchers have considered the coordination of flexible sources and loads to reduce the impact of uncertainty. Reference [16] proposed probabilistic optimal reactive power planning with the coordination of RDGs and loads to reduce the influence of uncertainty. Reference [17] used ESSs to reduce the uncertainty caused by fluctuations in PVs. However, the aforementioned measures did not consider the flexibility of the network.

The flexibility of the adjustment to the network structure is improved with the connection of a feeder terminal unit, which can accomplish distribution network reconfiguration (DNR) [18]-[21] in real time. In addition, with the application and promotion of power electronic equipment in ADSs, AC/DC hybrid ADSs based on voltage source converters (VSCs) are emerging; they realize a flexible and controllable power flow via soft open points (SOPs) [22], [23] and DC links [24], [25]. Moreover, dynamic thermal rating (DTR) technology [26], [27], which has been used in transmission systems, can be used in AC/DC hybrid ADSs to increase the flexible transmission capacity of the network. Such flexibilities in the structure, power flow, and capacity of the ADS cannot be disregarded, and several researchers have considered some of these issues. The first group of researchers utilized mixed-integer programming [18], [19] and heuristic al-

gorithms [20], [21] to implement DNR in an AC distribution network. The second group of researchers expanded a pure AC grid to an AC/DC hybrid ADS: ① [22], [23] transformed the tie line into an SOP in the ADS, built an SOP quadratic programming model, and realized real-time control of its active and reactive power; ② [24], [25], [28]-[30] established a quadratic programming model for AC/DC hybrid ADSs and realized optimal control of the radial structure in consideration of new energy fluctuations [28] and microgrid clusters [29]. This model was also applied to the optimal operation of a multi-DC interconnected ADS [30] and planning field [24], [25]. The third group of researchers, used DTR technology combined with a microgrid [26] and PVs [27], and achieved safe and economical operation of the ADS. Although the literature has considered some aspects of the flexibility of the ADS, a model and solution for comprehensive co-optimization still must be determined.

The optimized operation of dispatchable resources in an AC/DC hybrid ADS occurs on different time scales and must be separately considered. For example, DNR and an ESS cannot be frequently implemented, typically at the hour level at best [31], whereas the dispatch of a static var compensator (SVC) and an SOP is within minutes [23], generally 5-15 min at best. Moreover, the input data (the predicted values of the RDGs and load are regarded as the input data for dispatching) at different time scales affect the scheduling optimization results. Essentially, the longer time interval results in a greater error between the input data and actual value and, thus, the less accurate dispatching result based on these input data. Nonetheless, a shorter time interval requires more data and results in the lower solution efficiency and more unstable system. Some researchers have built multiscale optimal scheduling models to solve the above problems. Multiscale scheduling models have been established for distributed generation (DG) [32], on-load tap changers (OLTCs) [33], and commercial buildings with virtual energy storage [34] in the AC power grid. Two-stage scheduling for AC/DC hybrid ADSs considering DG and electric vehicle (EV) coordination [35] and ESSs [36] has been realized. However, the above studies did not consider the objective error between the actual operation and optimization plan. Therefore, a more sophisticated framework that considers all aforementioned aspects is necessary for an ADS to achieve an optimal state. For clarity, Table I compares the functionalities of the proposed model with those in previous studies, and Table II summarizes the differences between the models in previous studies and the proposed model. The two tables indicate several important deficiencies, which are as follows.

1) A wide majority of papers, which focused on the network flexibility of AC/DC hybrid ADSs, did not build a comprehensive model, particularly considering the DNR, SOP, and DTR together, which may allow the ADS to be safer and more economic, and accept more RDGs.

2) The dispatching framework has not balanced the contradiction between economic and safety dispatching; in particular, it has not achieved a balance between the maximum number of accommodated RDGs and the voltage stability.

TABLE I  
FUNCTIONALITIES OF MODEL PROPOSED IN THIS PAPER AND THOSE IN PREVIOUS STUDIES

Functionality	DNR [18]-[22], [26], [28]	SOP [22], [23]	DTR [26], [27]	AC/DC [24], [25], [28]-[30]	Proposed model
Increased RDG accommodation		✓	✓	✓	✓
Reconfigurable architecture	✓				✓
Real-time power control		✓		✓	✓
Expanded transfer capability			✓		✓

TABLE II  
DIFFERENCES BETWEEN MODELS IN PREVIOUS STUDIES AND PROPOSED MODEL

Difference	Reference	Proposed model
Single time scale	[21]	
Day-ahead & real-time	[28], [32], [33], [35], [37]	
Multiple time scales	[34]	✓
Minimized network loss and RDG dropout (economic dispatch)	[21], [28], [34], [35]	✓
Minimized network loss and voltage fluctuation (safety dispatch)	[32], [33], [36], [38]	✓

3) With the increase in dispatchable resources in AC/DC hybrid ADSs, the time scales of different resources and the dispatching framework need to be further refined. Moreover, the error between the actual operation and optimal plan caused by model mismatches must be solved using the framework.

Thus, a novel two-stage optimal dispatching framework for comprehensive cooperative AC/DC hybrid ADSs is proposed herein. The contributions of this study are summarized as follows.

1) A comprehensive cooperative ADS model that considers DNR, SOPs, DTR, and AC/DC hybridization is proposed. This model can release the line capacity, reduce losses, and improve the penetration rate of RDGs.

2) A novel two-stage framework for an AC/DC hybrid ADS, which considers the aforementioned dispatchable resources applied at different time scales, is introduced. The day-ahead dispatch outputs the hour-level optimization for DNR and the ESSs. The intraday dispatch provides a minute-level optimization of the remaining dispatchable resources. To further reduce the operation frequency of DNR, a time consolidation method based on Fisher segmentation is introduced. A threshold is set to check the difference between the day-ahead and intraday forecasts of the RDGs and the load to determine whether to start the intraday dispatch.

3) The intraday dispatch is decomposed into two parts, namely, the rolling-plan and real-time feedback dispatches, to overcome the deviation between the actual operation and optimization results, and accomplish economic and safety dispatching. The rolling-plan dispatch has the same objective

(to minimize the network loss and RDG dropout) as the day-ahead dispatch but optimizes for the next hour instead of a day. The rolling-plan dispatch is only implemented for the first 15 min in the above optimal scheduling result and it continues to optimize for the next hour and rolls again. Once an overvoltage is detected in the next hour of the rolling-plan dispatch, the aforementioned plan is reoptimized through safety dispatching, i.e., minimizing the network loss and voltage fluctuation. Real-time feedback dispatch divides the 15 min operation in the rolling-plan dispatch into three steps for execution (5 min each). The goal of this execution strategy is to follow the rolling-plan dispatch and minimize changes in the decision variables. The optimized value is replaced with the measured result to form closed-loop feedback after each step is completed to allow eliminating the error in each step.

The remainder of this paper is organized as follows. In Section II, the two-stage dispatching framework for AC/DC hybrid ADSs is presented. In Sections III and IV, the details of the day-ahead and intraday dispatches and solutions are described, respectively. In Section V, simulation and discussion are presented. Finally, this paper is concluded in Section VI.

## II. TWO-STAGE DISPATCHING FRAMEWORK FOR AC/DC HYBRID ADSs

In consideration of the cost, lines with numerous DC sources can first be transformed into DC feeders, and some tie lines in an AC distribution system can be gradually replaced with SOPs. The connection between the AC and DC grids uses a VSC, as shown in Fig. 1. Similar to an AC distribution network, the AC/DC hybrid ADS is still a loop design but operates in a radial manner. Accordingly, a model for AC/DC hybrid ADSs is presented in this section along with a two-stage dispatching framework to realize the optimal operation of decision variables at different time scales.

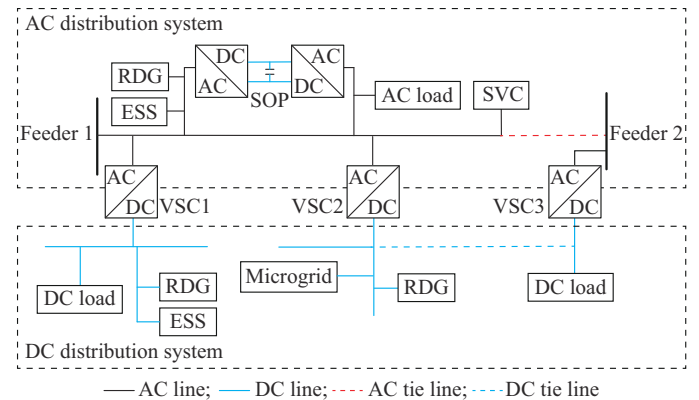


Fig. 1. Typical structure of an AC/DC hybrid ADS.

### A. Modeling of AC/DC Hybrid ADSs

Figure 1 shows that an AC/DC hybrid ADS consists of three parts: AC distribution system, DC distribution system, and connection. This paper proposes a framework to accommodate uncertainty rather than focusing on a forecast of the uncertainty. Thus, the predicted output values of the RDGs

and load are regarded as the input data. Focus has been placed on the power flow of the ADS and the flexibility of the network such as power flow for AC/DC conversion, SOP, DTR, and DNR.

### 1) Modeling Power Flow

The DisFlow model [37] is used to describe the power flow in the AC grid in an AC/DC hybrid ADS. Assuming that  $I^2 = \tilde{I}$  and  $U^2 = \tilde{U}$  to simplify the equations, the DisFlow model is obtained as follows.

$$\begin{cases} \sum_{a \in \varphi_i^{AC}} P_{ia,t} = \sum_{j \in \Phi_i^{AC}} (P_{ji,t} - \tilde{I}_{ji,t} R_{ji}) + P_{i,t}^{InAC} \\ \sum_{a \in \varphi_i^{AC}} Q_{ia,t} = \sum_{j \in \Phi_i^{AC}} (Q_{ji,t} - \tilde{I}_{ji,t} X_{ji}) + Q_{i,t}^{InAC} \end{cases} \quad \forall i, j, a \in \varpi^{AC} \quad (1)$$

$$\begin{cases} P_{i,t}^{InAC} = P_{i,t}^{sub} + P_{i,t}^{RDG} + P_{i,t}^{ESSout} - P_{i,t}^{ESSin} - P_{i,t}^{load} - P_{i,t}^{VSC} - P_{i,t}^{SOP} \\ Q_{i,t}^{InAC} = Q_{i,t}^{sub} + Q_{i,t}^{RDG} + Q_{i,t}^{SVG} - Q_{i,t}^{load} - Q_{i,t}^{VSC} - Q_{i,t}^{SOP} \end{cases} \quad (2)$$

s.t.

$$\tilde{U}_{i,t} = \tilde{U}_{j,t} - 2(R_{ji} P_{ji,t} + X_{ji} Q_{ji,t}) + (R_{ji}^2 + X_{ji}^2) \tilde{I}_{ji,t} \quad (3)$$

$$\tilde{I}_{ji,t} \tilde{U}_{j,t} = P_{ji,t}^2 + Q_{ji,t}^2 \quad (4)$$

The power flow in the DC grid based on the DisFlow model [37] is as follows.

$$\sum_{b \in \varphi_n^{DC}} P_{nb,t} = \sum_{m \in \Phi_n^{DC}} (P_{mn,t} - \tilde{I}_{mn,t} R_{mn}) + P_{n,t}^{InDC} \quad \forall m, n, b \in \varpi^{DC} \quad (5)$$

$$P_{n,t}^{InDC} = P_{n,t}^{RDG} + P_{n,t}^{ESSout} - P_{n,t}^{ESSin} - P_{n,t}^{load} + P_{n,t}^{VSC} \quad (6)$$

s.t.

$$\tilde{U}_{n,t} = \tilde{U}_{m,t} - 2R_{mn} P_{mn,t} + R_{mn}^2 \tilde{I}_{mn,t} \quad (7)$$

$$\tilde{I}_{mn,t} \tilde{U}_{m,t} = P_{mn,t}^2 \quad (8)$$

The variables have the same meanings as those in the AC grid, except for  $P_{n,t}^{VSC}$ , which represents the power flow injected into the  $n^{\text{th}}$  node from the AC grid through the VSC. Some limits exist for the voltage and current, such as:

$$U_{\min}^{AC} \leq U_{i,t} \leq U_{\max}^{AC} \quad (9)$$

$$U_{\min}^{DC} \leq U_{n,t} \leq U_{\max}^{DC} \quad (10)$$

$$|S_l| \leq |S_{l,\max}| \quad \forall l \quad (11)$$

Equations (9) and (10) represent the bus voltage limits of the AC and DC grids, respectively. Equation (11) is the line capacity limit, which can be calculated on the basis of either the static thermal rating (STR) or DTR [26].

RDGs, ESSs, and the SVC, which can be dispatched, are connected to the ADS. They should satisfy the following constraints, the details of which can be found in [28].

$$0 \leq P_{i,t}^{RDG} \leq P_{i,t}^{RDG,f} \quad (12)$$

$$Q_{i,t}^{RDG} \leq P_{i,t}^{RDG} \tan \theta_{RDG} \quad (13)$$

$$0 \leq P_{n,t}^{RDG} \leq P_{n,t}^{RDG,f} \quad (14)$$

$$E_{s,t}^{out} + E_{s,t}^{in} \leq 1 \quad \forall s \in \varpi^{AC} \cup \varpi^{DC} \quad (15)$$

$$0 \leq P_{s,t}^{ESSout} \leq E_{s,t}^{out} P_{\max}^{ESS} \quad (16)$$

$$0 \leq P_{s,t}^{ESSin} \leq E_{s,t}^{in} P_{\max}^{ESS} \quad (17)$$

$$W_{s,t+1}^{ESS} = W_{s,t}^{ESS} + \alpha P_{s,t}^{ESSin} \Delta t - \beta P_{s,t}^{ESSout} \Delta t \quad (18)$$

$$0.2 W_{\max}^{ESS} \leq W_{s,t}^{ESS} \leq 0.9 W_{\max}^{ESS} \quad (19)$$

$$Q_{\min}^{SVC} \leq Q_{i,t}^{SVC} \leq Q_{\max}^{SVC} \quad (20)$$

Equations (12) and (13) are the limits of the RDGs connected to the AC grid. Equation (14) indicates the limits of the RDGs connected to the DC grid. Equation (15) is the action limit for ESS charging or discharging. Equations (16) and (17) are the charging-rate limits of the ESS. Equations (18) and (19) represent the capacity limits of the ESS. Equation (20) denotes the reactive power limit of the SVC. Thus, the decision variables are  $X^{RDG} = [P_{s,t}^{RDG}, Q_{s,t}^{RDG}]$ ,  $X^{ESS} = [P_{s,t}^{ESS}]$ , and  $X^{SVC} = [Q_{i,t}^{SVC}]$ .

### 2) Modeling VSC

The power flow injected into the DC grid is the power flowing out of the AC grid through the VSC. Thus, the VSC model consists of an equivalent resistance, reactance, and ideal VSC, as shown in Fig. 2. The active/reactive power constraint of the VSC is given by (21), and the capacity constraint is given by (22).

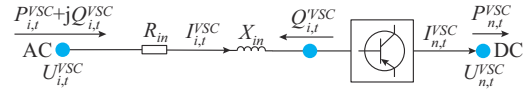


Fig. 2. VSC model.

$$\begin{cases} P_{i,t}^{VSC} - \tilde{I}_{i,t}^{VSC} R_{in} = P_{n,t}^{VSC} \\ Q_{i,t}^{VSC} - \tilde{I}_{i,t}^{VSC} X_{in} = -Q_{i,t}^{VSC} \\ P_{\min}^{VSC} \leq P_{i,t}^{VSC} \leq P_{\max}^{VSC} \\ Q_{\min}^{VSC} \leq Q_{i,t}^{VSC} \leq Q_{\max}^{VSC} \end{cases} \quad (21)$$

$$\sqrt{(P_{i,t}^{VSC})^2 + (Q_{i,t}^{VSC})^2} \leq S_{\max}^{VSC} \quad (22)$$

The VSC can control only any two of these quantities: the active power, reactive power, voltage on the AC side, and voltage on the DC side. The  $U_{dc}Q$  control [16] is chosen in this study; that is,  $Q_{i,t}^{VSC}$  and  $U_{n,t}^{VSC}$  are set to control  $P_{i,t}^{VSC}$ ,  $U_{i,t}^{VSC}$  through (21). Thus, the decision variables of the VSC are  $X^{VSC} = [P_{i,t}^{VSC}, U_{i,t}^{VSC}]$ .

### 3) Modeling SOP

The SOP, a flexible power electronic device, can be used as a dispatchable source to realize fast power control on both sides [23]. It is a symmetric structure consisting of two VSCs connected back-to-back, as shown in Fig. 3. The active/reactive power constraints of the SOP are presented in (23), and the capacity constraints are expressed in (24).

$$\begin{cases} P_{i,t}^{SOP} + P_{j,t}^{SOP} = 0 \\ Q_{\min}^{SOP} \leq Q_{i,t}^{SOP} \leq Q_{\max}^{SOP} \\ Q_{\min}^{SOP} \leq Q_{j,t}^{SOP} \leq Q_{\max}^{SOP} \end{cases} \quad (23)$$

$$\begin{cases} \sqrt{(P_{i,t}^{SOP})^2 + (Q_{i,t}^{SOP})^2} \leq S_{\max}^{SOP} \\ \sqrt{(P_{j,t}^{SOP})^2 + (Q_{j,t}^{SOP})^2} \leq S_{\max}^{SOP} \end{cases} \quad (24)$$

The SOP controls two VSCs. In general, the control method is as follows. One VSC realizes DC voltage control, whereas the other VSC realizes power control, i.e.,  $PQ-U_{dc}Q$  control [23]. Thus, the decision variables of the SOP are

$$\mathbf{X}^{SOP} = [P_{i,t}^{SOP}, Q_{i,t}^{SOP}, P_{j,t}^{SOP}, Q_{j,t}^{SOP}]$$

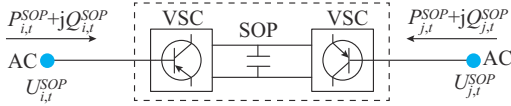


Fig. 3. Two-port SOP model.

#### 4) Modeling DTR

The maximum line capacity is typically calculated using a fixed set of conservative weather assumptions (STR value), which leads to conservative operational limits. If real-time weather conditions are considered, the maximum line capacity should be regarded as the independent constraint in (25), which is called the DTR value.

$$S_{l,\max} = \sqrt{3} UI_{DTR} = \sqrt{3} U \sqrt{[Q_c(T_a, T_c, V_w, \theta_w) + Q_r(T_a, T_c) - Q_s] / R(T_c)} \quad (25)$$

Thus, (25) is the line capacity considering the DTR value.  $I_{DTR}$  is not a decision variable but a variable based on micro-meteorology. With large-scale access to RDGs, the line is more likely to be overloaded, and the use of DTR technology can potentially improve the practicality and flexibility of the capacity at certain special time (such as during overloading).

#### 5) Modeling DNR

The variable  $Z_{ij,t} \in \{1, 0\}$  is introduced to describe the on-off state of a branch, and a large number ( $M$ ) [18] is input into (3) to establish the upper and lower bounds, as follows.

$$\begin{cases} \tilde{U}_{i,t} \leq \tilde{U}_{j,t} - 2(R_{ji}P_{ji,t} + X_{ji}Q_{ji,t}) + (R_{ji}^2 + X_{ji}^2)\tilde{I}_{ji,t} + M(1 - Z_{ij,t}) \\ \tilde{U}_{i,t} \geq \tilde{U}_{j,t} - 2(R_{ji}P_{ji,t} + X_{ji}Q_{ji,t}) + (R_{ji}^2 + X_{ji}^2)\tilde{I}_{ji,t} - M(1 - Z_{ij,t}) \end{cases} \quad (26)$$

If  $Z_{ij,t} = 1$ , i.e., branch  $(i, j)$  is closed, (26) equals (3). Otherwise, if  $Z_{ij,t} = 0$ , i.e., branch  $(i, j)$  is opened,  $I_{ij,t}^2 = 0$ . Thus, (26) changes into  $M \geq |U_{i,t}^2 - U_{j,t}^2|$ . Considering that  $|U_{\max}^2 - U_{\min}^2| \geq |U_{i,t}^2 - U_{j,t}^2|$ , herein,  $M = |U_{\max}^2 - U_{\min}^2|$  is set to balance the contradiction between the solution rate and the Big  $M$  method requirements. The current constraint is expressed as follows.

$$0 \leq \tilde{I}_{ij,t} \leq Z_{ij,t} \tilde{I}_{ij,t} \leq Z_{ij,t} \tilde{I}_{\max} \quad (27)$$

Therefore, the decision variable for DNR is the topology.

Given that the topology after DNR should be radial, the limits of the radial topology are as follows.

$$\begin{cases} K_{ij,t} + K_{ji,t} = Z_{ij,t} & i, j = 1, 2, \dots, n \\ \sum K_{ij,t} = 1 & i, j = 1, 2, \dots, n \\ K_{ij,t} = 0 \\ K_{ji,t} \in \{0, 1\} \\ K_{ji,t} \in \{0, 1\} \end{cases} \quad (28)$$

When power flows from node  $i$  to node  $j$ ,  $K_{ij,t} = 1$ , and node  $i$  is considered superior to node  $j$ . If the power flow is reversed,  $K_{ji,t} = 1$ . If no power flow occurs between the nodes,  $K_{ij,t} = K_{ji,t} = 0$ . Thus, the first term limit is that only one of  $K_{ij,t}$  and  $K_{ji,t}$  can be 1. The second term limit is that all nodes except the one connected to the substation have only one superior node. The third term limit is that any node

connected to the substation does not have a superior node.

#### B. Dispatching Framework for AC/DC Hybrid ADSs

Considering that the optimization operations of dispatchable resources in an ADS are applied at different time scales, herein, a two-stage dispatch framework is proposed, which contains day-ahead dispatch and intraday dispatch. This framework divides the time scale into hour (day-ahead dispatch) and minute (intraday dispatch) levels to meet the requirements of the controllable variables in the ADS at different time scales. The intraday dispatch (15 min) is divided into three execution steps (5 min each) to reduce the deviation between the actual operation and optimal plan. The framework is illustrated in Fig. 4.

The day-ahead dispatch optimizes the operations for the next 24 hours using input data with a time slot of 1 hour  $\Delta t_a$ . It maximizes the topology  $\mathbf{X}^{ESS}$  and other controllable variables, namely  $\mathbf{X}^{RDG}$ ,  $\mathbf{X}^{SVC}$ ,  $\mathbf{X}^{VSC}$ ,  $\mathbf{X}^{SOP}$ , by setting an economic goal (i. e., minimizing the system loss and RDG waste). To reduce the effect of DNR on the system, the day-ahead dispatch divides 24 hours into several periods, and each period only performs DNR.

Given that the forecasted data used as the input data for the day-ahead dispatch may be very close to the intraday input data (i. e., the fluctuations in the RDGs and load are small), the intraday dispatch is not required in that situation. Therefore, the framework performs a judgment every 15 min in day-ahead dispatch to determine whether the current moment enters the intraday schedule. This judgment is based on the difference between the day-ahead and intraday input data.

The intraday dispatch is divided into two parts: rolling-plan dispatch and real-time feedback dispatch [38]. The dispatch for DNR and  $\mathbf{X}^{ESS}$  is obtained from the day-ahead dispatch and not rescheduled during the intraday dispatch. The rolling-plan dispatch uses input data with a time slot of 15 min  $\Delta t_{ip}$  to optimize operations in the next 1 hour with the same goal as the day-ahead dispatch. Once an overvoltage occurs in the dispatching plan, the safety dispatch with the smallest voltage fluctuation and grid loss is adopted to re-optimize the rolling-plan dispatch.

The rolling-plan dispatch can optimize the remaining dispatchable resources in multiple stages; however, it only executes the optimization results of the first stage. For example, it optimizes the next 1 hour in four stages (each  $\Delta t_{ip}$  is a stage), as shown in Fig. 4, and it only executes the first  $\Delta t_{ip}$ . Subsequently, the optimization of the rolling-plan dispatch continues in the next optimization cycle. Therefore, the superposition of errors caused by the changes in the input data in multiple stages can be prevented.

In addition, the framework refines the execution of the first stage, called the real-time feedback dispatch, to resolve the deviation of the actual operation from the plan. In the real-time feedback dispatch, the tie-line power between the ADS and upper grid follows the first step of the rolling-plan dispatch and minimizes the changes in the controllable variables. Finally, the real-time feedback dispatch replaces the optimized values with the measured data in 5 min, thus forming closed-loop feedback to reduce bias.

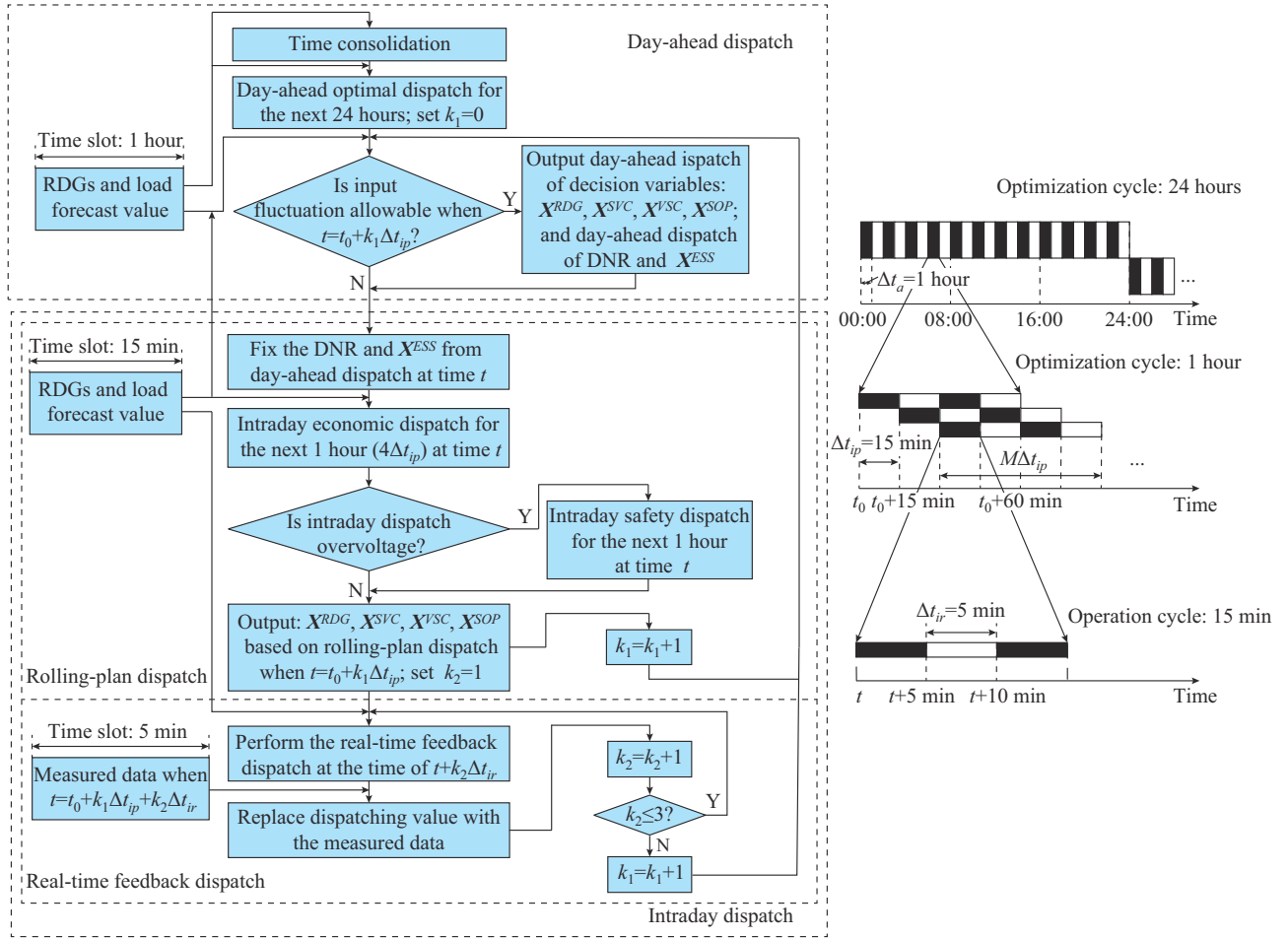


Fig. 4. Dispatching framework for AC/DC hybrid ADSs.

In this regard, the framework optimizes dispatchable resources into an appropriate time scale and minimizes the effect of uncertainty through the real-time feedback dispatch to ensure the economic and safe operation of the ADS. The details are presented in the following sections.

### III. DAY-AHEAD DISPATCH AND SOLUTION

The forecasting data of the RDGs and load in a 1-hour time slot are used as input data for the day-ahead dispatch. Combined with the AC/DC hybrid ADS model presented in Section II-A, the day-ahead dispatch of the decision variables is obtained. In addition, the relaxation from the initial model to a second-order cone programming (SOCP) problem is presented in this section. Finally, time consolidation is proposed to reduce the DNR time.

#### A. Objective of Day-ahead Dispatch

An ADS can realize the active control of resources in a network and maximize RDG access. Thus, the objective is to minimize the network loss and RDG dropout as follows.

$$\min \sum_{t=1}^{24} (C_l P_{l,t} + \sum C_{RDG} P_{RDG,t}^{cut}) \quad (29)$$

$$P_{l,t} = \sum_{\forall i,j \in \varpi^{AC}} \Delta t_a (\tilde{I}_{ji,t} R_{ji}) + \sum_{\forall m,n \in \varpi^{DC}} \Delta t_a (\tilde{I}_{mn,t} R_{mn}) \quad (30)$$

$$P_{RDG,t}^{cut} = \sum \Delta t_a \sum_{i \in \varpi^{AC}} (P_{i,t}^{RDG,f} - P_{i,t}^{RDG}) + \sum \Delta t_a \sum_{n \in \varpi^{DC}} (P_{n,t}^{RDG,f} - P_{n,t}^{RDG}) \quad (31)$$

Note that the losses of the VSC and SOP are not considered here. If they are considered, the loss (i.e.,  $C_{sop} \lambda S^{sop} + C_{vsc} \mu S^{vsc}$ ) is only added to (29). Here,  $\lambda$  and  $\mu$  are the loss coefficients of the SOP [22] and VSC [37], respectively.

#### B. Solving Day-ahead Dispatch

The day-ahead dispatch, i.e., (30), with the limits in (1), (3)-(5), (7)-(24), and (26)-(28), is a mixed-integer nonconvex and nonlinear problem. It can be transformed into an SOCP problem via convex relaxation [18] as follows.

- 1) The constraints in (4) and (8) can be relaxed to:

$$\begin{cases} 2P_{ji,t} \\ 2Q_{ji,t} \\ \tilde{I}_{ji,t} - \tilde{U}_{j,t} \end{cases} \leq \tilde{I}_{ji,t} + \tilde{U}_{j,t} \quad \forall i,j \in \varpi^{AC} \quad (32)$$

$$\begin{cases} 2P_{mn,t} \\ \tilde{I}_{mn,t} - \tilde{U}_{n,t} \end{cases} \leq \tilde{I}_{mn,t} + \tilde{U}_{n,t} \quad \forall m,n \in \varpi^{DC} \quad (33)$$

- 2) The capacity constraints of the VSC and SOP, i.e., (22) and (24), are changed into cone rotation constraints as follows.

$$\left\| \begin{matrix} P_{i,t}^{VSC} \\ Q_{i,t}^{VSC} \end{matrix} \right\|_2 \leq S_{\max}^{VSC} \quad \forall i, j \in \varpi^{AC} \quad (34)$$

$$\left\| \begin{matrix} P_{i,t}^{SOP} \\ Q_{i,t}^{SOP} \end{matrix} \right\|_2 \leq S_{\max}^{SOP} \quad \forall i \in \varpi^{AC} \quad (35)$$

Thus, the initial day-ahead dispatch is transformed into (36).

$$\left\{ \begin{array}{l} \text{Objective: (29)} \\ \text{s.t.} \\ \text{Power flow limits: (1)-(8), (26)-(28), (32), (33)} \\ \text{Voltage and current limits: (9)-(11)} \\ \text{RDG limits: (12)-(14)} \\ \text{ESS and SVC limits: (15)-(20)} \\ \text{VSC and SOP limits: (21), (23), (34), (35)} \end{array} \right. \quad (36)$$

This equation is an SOCP problem and can be solved using commercial software such as CPLEX and GUROBI.

### C. Time Consolidation

If the DNR is considered hourly, finding a solution to (36) becomes time-consuming and affects the system frequency. If the changes in the RDG output and load between two consecutive hours are minimal, no DNR is required, thereby reducing the aforementioned effect and improving the solving rate. Thus, herein, time consolidation is conducted and DNR is performed at a divided time. Further, optimal merging is proposed at the temporal order using Fisher segmentation [39]. The details are as follows.

1) An equivalent load is determined. The forecast for the RDGs is regarded as a negative load and added to the power demand. The equivalent load is obtained as  $\{L_{0,1}, L_{1,2}, \dots, L_{d,d+1}, \dots, L_{23,24}\}$  in the day-ahead dispatch. Here,  $L_{d,d+1}$  is the equivalent load demand of the ADS between hours  $d$  and  $d+1$ .

2) Dispersion is determined. The equivalent loads are assumed to be divided into  $k$  segments, and  $D = \{d_0, d_1, \dots, d_k\}$  is the set of time-dividing points, where  $d_0 = 0$ ,  $d_k = 24$ . Thus, the equivalent loads are divided into  $\{L_{d_0,1}, L_{1,2}, \dots, L_{d_1-1,d_1}\}$ ,  $\{L_{d_1,d_1+1}, L_{d_1+1,d_1+2}, \dots, L_{d_2-1,d_2}\}$ ,  $\dots$ ,  $\{L_{d_{k-1},d_{k-1}+1}, \dots, L_{23,d_k}\}$ . The dispersion (called a similar diameter) between the equivalent loads within the  $k^{\text{th}}$  segment and its average are as follows.

$$D(d_k) = \sum_{\zeta=d_{k-1}}^{d_k-1} (L_{\zeta,\zeta+1} - \bar{L}_{d_{k-1},d_k})^2 \quad (37)$$

$$\bar{L}_{d_{k-1},d_k} = \sum_{\zeta=d_{k-1}}^{d_k-1} L_{\zeta,\zeta+1} / (d_k - d_{k-1}) \quad (38)$$

Essentially, the smaller the  $D(d_k)$  is, the smaller the dispersion in the data within a time segment will be.

3) Time division is determined. The segments, in which the dispersion in the equivalent load within each segment is the smallest and that between segments is the largest, are identified as follows.

$$E(24, k) = \min \sum_{k=1}^x D(d_k) \quad (39)$$

Equation (39) indicates that the 24 hours of the day-ahead

dispatch are divided into  $x$  segments on the basis of minimizing the change in the equivalent load over the same period (equal to maximizing the gap between different periods [39]). The solving method can be found in [39].

## IV. INTRADAY DISPATCH AND SOLUTION

The forecasts of the RDGs and load in 15 min are used as the input data for the intraday dispatch. The dispatch for DNR and the ESSs is fixed with the day-ahead dispatching result; thus, the intraday decision variables are  $X = [X^{RDG}, X^{SVC}, X^{VSC}, X^{SOP}]$ . The rolling-plan dispatch builds an optimal dispatching plan for  $X$  for the next hour but only executes the first 15 min. The real-time feedback dispatch divides 15 min into three 5-min steps and uses the measured data as the input after each step to reduce the deviation between actual operation and the optimized dispatching plan.

### A. Objective of Rolling-plan Dispatch

#### 1) Economic Dispatch

The intraday rolling-plan dispatch smooths the large fluctuations in the RDGs and loads to achieve economic dispatch, which has the same objective as the day-ahead dispatch, as shown in (40). The differences between the two are as follows. ① The input data of the rolling-plan dispatch include a 15-min time slot, which is more accurate. ② The optimization period is 1 hour rather than 1 day, which is more suitable for the fluctuations in the RDGs and load. ③ The dispatch for DNR and the ESSs is not optimized in the rolling-plan dispatch.

$$\min \sum_{t=t_0}^{4\Delta t_{ip}} (C_l P_{l,t} + \sum C_{RDG} P_{RDG,t}^{cut}) \quad (40)$$

where  $4\Delta t_{ip}$  is the optimization cycle, i.e., 1 hour in this study; and  $\Delta t_{ip}$  is the AC time slot of the rolling-plan dispatch, i.e., 15 min. The other variables are the same as those in (29).

#### 2) Safety Dispatch

In the rolling-plan dispatch, the overvoltage caused by the fluctuations in the RDGs must be solved because they become increasingly serious with the increase of RDG penetration [23]. Therefore, once the rolling-plan dispatch detects an overvoltage, the safety dispatch is adopted to reoptimize the rolling-plan dispatch as follows.

$$\min \sum_{t=t_0}^{4\Delta t_{ip}} \left( P_{l,t} + \sum_{\forall u \in \varpi^{AC} \cup \varpi^{DC}} |\tilde{U}_{s,t} - 1| \right) \quad (41)$$

Equation (41) indicates the minimum voltage fluctuations.

To maintain voltage stability, the determination of an overvoltage does not use a threshold [0.93, 1.07] but a margin [37], i.e.,  $U_{s,t} \in [1 - \tau, 1 + \tau]$ ,  $\tau \in [0, 0.07]$ .

In this manner, the rolling-plan dispatch provides a four-step optimal plan for the next hour at 15-min intervals. To prevent disturbances from accumulating in the four steps, the rolling-plan dispatch only executes the first 15 min (first step) [38] and then reoptimizes the next hour plan at  $t = t_0 + \Delta t_{ip}$ .

### B. Objective of Real-time Feedback Dispatch

The severe fluctuations in the input data caused by sudden meteorological changes can be addressed by shortening the optimization cycle and time slot. However, the actual operation of an ADS may not be completely consistent with the optimized scheme because of acquisition and model errors. Therefore, the real-time feedback dispatch decomposes the first step of the rolling-plan dispatch (15 min) into three 5-min steps and feeds the measured data back to each step, thereby dynamically adjusting the decision variables.

The real-time feedback dispatch is not meant to change the rolling-plan dispatch; instead, it is meant to adjust the output of the decision variables within a shorter time scale on the basis of the measured data. Therefore, the objective of each 5-min step is to minimize the changes in the decision variables and reduce the effect on the upper power grid caused by fluctuations, which is shown as follows.

$$\min \{ \|Y - Y_{t+\Delta t}^{ref}\|_2 + \|\Delta X\|_2 \} \quad (42)$$

After each step is completed, the optimization plan for the decision variables is replaced with the measured data. Thus, the decision variables are corrected in time through the feedback of the measured data to form closed-loop optimal control. After the three 5-min steps are completed, a day-ahead dispatch is performed to determine whether the intraday dispatch should enter at  $t + \Delta t_{ip}$ . This cycle is repeated, as shown in Fig. 4.

### C. Solution for Intraday Dispatch

The intraday dispatch has the same constraints as the day-ahead dispatch but with different targets. Accordingly, it can also be relaxed to the SOCP model, as shown in (43), and solved as a day-ahead dispatch.

$$\left. \begin{array}{l} \text{Objective:} \\ (49) \text{ if choosing economic dispatch} \\ (50) \text{ if choosing safety dispatch} \\ (51) \text{ if choosing real-time feedback dispatch} \\ \text{s.t.} \\ \text{Power flow limits: (1)-(8), (26)-(28), (32), (33)} \\ \text{Voltage and current limits: (9)-(11)} \\ \text{RDG limits: (12)-(14)} \\ \text{ESS and SVC limits: (15)-(20)} \\ \text{VSC and SOP limits: (21), (23), (34), (35)} \end{array} \right\} \quad (43)$$

## V. SIMULATION AND DISCUSSION

To test the model and dispatching framework, two test systems, from simple to complex, have been built: ① a simple AC/DC hybrid test system; and ② a 51-node AC/DC hybrid ADS with RDGs, an SOP, an SVC, and ESSs. The proposed model is implemented with the YALMIP optimization toolbox [39] and MATLAB R2020a, and solved using CPLEX.

### A. Test Systems

Test system 1 is a simple AC/DC hybrid system that converts part of the AC overhead line into a DC line (called Line 2), as shown in Fig. 5. The parameters of the overhead

lines are provided in [26]. The other parameters are presented in [31].

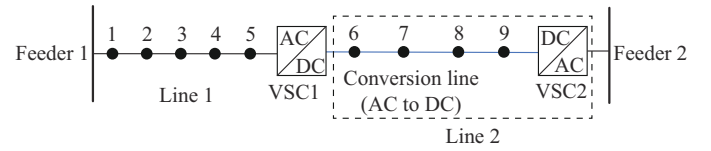


Fig. 5. Test system 1: simple AC/DC hybrid system.

Test system 2 is a 51-node AC/DC hybrid ADS formed by one IEEE 33-node AC grid [22] and three DC grids, as shown in Fig. 6. The capacity of the RDGs (including PVs and WTs) is 300 kW, and  $\tan \theta_{RDG} = 0.9$ . The reactive capacity of the VSC is  $\pm 300$  kvar, whereas the capacity of the SOP is  $\pm 3.0$  MW [22]. The active and reactive capacities of the VSC are set to be  $\pm 2.0$  MW and  $\pm 1.0$  Mvar, respectively [30]. Further,  $C_l = 100$  CNY/MWh, and  $C_{RDG} = 400$  CNY/MWh. The parameters and loads of the AC grid can be found in [22]; the branch parameters of DC grid and loads of the test system 2 are listed in Tables III and IV, respectively. Four ESSs were connected. ESS1 and ESS4 have a capacity of 1.8 MWh and a charging/discharging power rating of 300 kW. The other two have a capacity of 1.4 MWh and a power rating of 240 kW. The initial stage of the ESSs has a capacity of 30%.

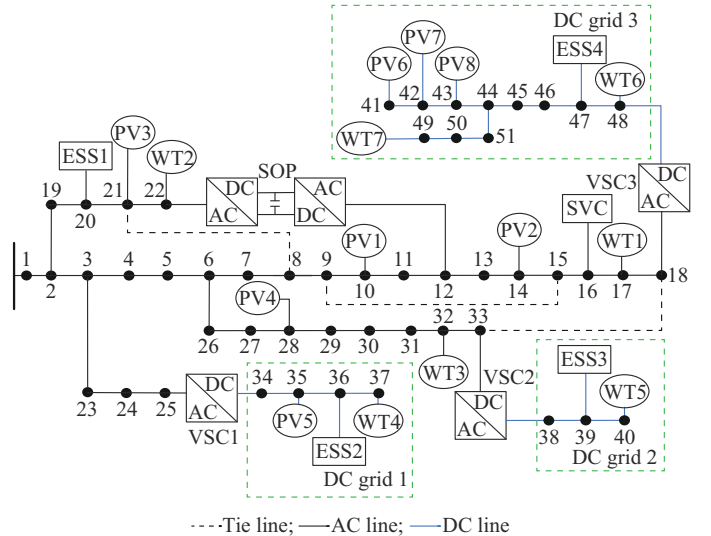


Fig. 6. Test system 2: 51-node AC/DC hybrid ADS.

TABLE III  
BRANCH PARAMETERS OF DC GRID OF TEST SYSTEM 2

From bus	To bus	$R$ ( $\Omega$ )	From bus	To bus	$R$ ( $\Omega$ )
34	35	0.493	44	45	0.541
35	36	0.366	45	46	0.591
36	37	0.381	46	47	0.378
38	39	0.819	47	48	0.746
39	40	0.187	49	50	0.708
41	42	0.711	50	51	0.683
42	43	1.044	44	51	1.289
43	44	0.374			

TABLE IV  
 LOADS IN DC GRID OF TEST SYSTEM 2

Bus	Power (kW)						
34	100	40	90	45	40	50	60
35	90	41	80	46	40	51	40
37	60	42	80	47	80		
38	60	43	80	48	100		
39	100	44	80	49	80		

### B. Maximum Transfer Capability

The maximum transfer capability was determined primarily by the line thermal and node voltage limits [37]. The influences on the maximum transfer capability in terms of two flexibilities, i.e., the DTR and AC/DC hybrid, are discussed. Three situations in test system 1 are compared: ① a pure AC system (only the power supply of Feeder 1); ② an AC/DC hybrid system; and ③ an AC/DC hybrid system that applies the DTR. The lowest node voltages at different load levels are shown in Fig. 7. The inset graph shows the transmission capability of the line for 48 hours of weather conditions in Shandong province, China, in 2019. DTR1 and DTR2 are two different constraints for test system 1 based on the minimum and maximum values of the DTR over 48 hours. The microclimate data for DTR1 and DTR2 are listed in Table V.

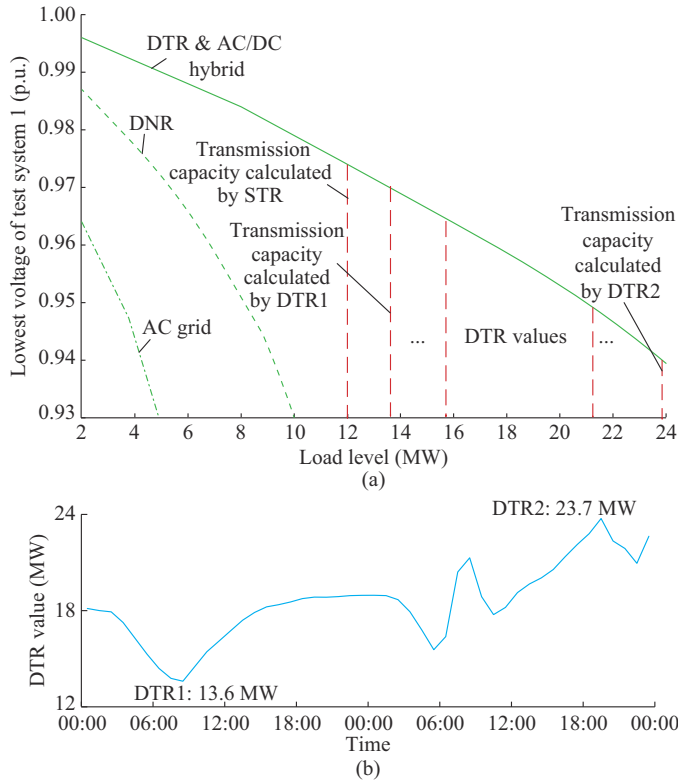


Fig. 7. Lowest node voltage at different load levels in test system 1. (a) Lowest node voltage. (b) DTR value.

As shown in Fig. 7, the pure AC grid could transfer only 4.9 MW because the lowest node voltage (Node 9) of the system is 0.93 p.u., which is considerably lower than the

transfer capacity of the AC lines calculated via the STR (12 MW). At this point, Feeder 2 is not connected. If the DNR is implemented in the AC system, i.e., Feeder 2 is connected, it could transfer 10.06 MW, where the node with the lowest voltage is changed to Node 6. Further, the loss is up to 32.49%. This phenomenon is possible because the active power and reactive power are supplied from the two feeders separately after Feeder 2 is connected, thereby providing sufficient reactive power to maintain voltage but causing the increase of loss. The AC/DC hybrid system could transfer considerably more energy compared with the AC system, as shown in Fig. 7, because the  $U_{dc}$  control of the VSC relaxes the voltage constraint by adjusting the reactive power in real time to ensure that the DC-side voltage is 1 p.u.. With the DTR, the line thermal limits are relaxed in accordance with different weather conditions, as shown in the inset graph in Fig. 7. The minimum (DTR1) and maximum (DTR2) transfer capacities are 2.78 and 4.83 times those of the pure AC system, respectively. In summary, the AC/DC hybrid system that applies a DTR can release the line capacity and node voltage limits. Thus, it is useful in emergency scenarios such as  $N-1$  failures and load surges.

 TABLE V  
 MICROCLIMATE DATA

No.	$V_w$ (m/s)	$\theta_w$ ( $^{\circ}$ )	$T_a$ ( $^{\circ}$ C)	$T_c$ ( $^{\circ}$ C)	DTR (MW)
STR	0.50	0	40.0	100	12.0
DTR1	1.36	12.60	18.7	100	13.6
DTR2	5.06	30.34	26.8	100	23.7

### C. System Loss and RDG Penetration

In this case, a complex system, i.e., test system 2, is considered and three models are compared: ① the model used in this study (No. 1); ② a model without an SOP (No. 2); and ③ a model without an SOP and a DNR (No. 3). The day-ahead input [18] (each RDG and load change are in the same proportion) and the equivalent load are shown in Fig. 8. To avoid the effect of frequent DNR,  $x=3$  is set, and the time interval of DNR is more than 3 hours. In accordance with Section III-C, the best consolidation time could be obtained: 00:00-10:00, 10:00-18:00, and 18:00-24:00. The results are compared in Table VI.

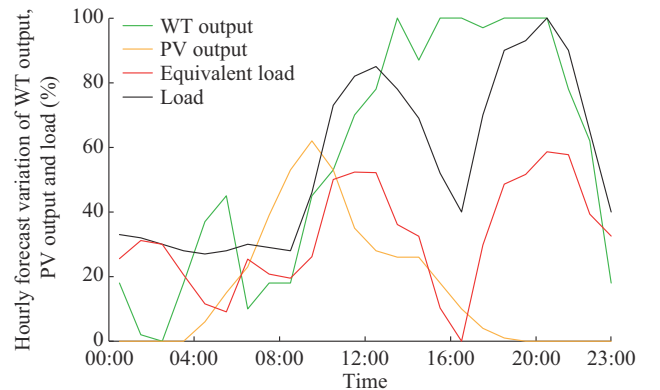


Fig. 8. Hourly forecasts of load, PV output, and WT output.

The power loss of the system is reduced by 25.9% (No. 1) and 13.4% (No. 2) compared with the No. 3 model. This is due to the following reasons. ① The power flow can be transferred at a large scale through DNR and has various directions. If DNR is absent, the power flow can only pass through a fixed topology, which may cause significant loss at the node and line near the upper grid. For example, at 05:00-07:00, a large amount of power provided by VSC3 flows into Node 33 through branches 33-18 because of DNR, thereby reducing the power demand of the branch where Node 33 is located in the upper power grid and decreasing losses. ② The SOP can adjust the active and reactive power and quickly respond to the fluctuations to maintain economic operation, whereas DNR can only change once in a time segment. For example, at 08:00-10:00, the active power of the SOP is from Nodes 22 to 12, whereas the others are opposite in the same time segment (00:00-10:00) to achieve optimal operation. By contrast, DNR could only choose one topology in the same segment, thus causing more losses than the SOP. In summary, DNR can optimize the power flow of the entire topology and entire day, whereas the SOP can optimize the power flow in the region where it is located in real time. The synergy between the two can reduce the loss better.

TABLE VI  
OPTIMAL DAY-AHEAD DISPATCH RESULTS

No.	Time division	Branch open	Power loss (kWh)
1	00:00-10:00	6-7; 10-11; 9-15	370.42
	10:00-18:00	6-7; 8-9; 9-15	
	18:00-24:00	6-7; 10-11; 9-15	
2	00:00-10:00	6-7; 13-14; 15-16	433.21
	10:00-18:00	6-7; 12-13; 9-15	
	18:00-24:00	7-8; 13-14; 15-16	
3			500.11

When the loads are light, the RDGs will change the power flow, thus raising the voltage of the access point and even causing an overvoltage. Herein, the load ratio is fixed to the minimum value for the entire day, i.e., 27%, thus causing the RDGs to output at the maximum, i.e., 100%, without considering the ESSs and SVC. This extreme case is considered to study the influence on RDG penetration. The highest voltages of test system 2 at different RDG penetration levels are shown in Fig. 9. The base case has the same structure as test system 2, but all the DC lines in test system 2 are reverted to AC lines.

Evidently, the highest voltage occurs at Node 41, and it increases to 1.07 p.u. when the maximum DG capacity of the base case is 186 kW (penetration level is about 55%). DNR could alleviate the overvoltage in the base case. When the maximum DG capacity increases to 240 kW (penetration level is approximately 71%), Node 41 experiences an overvoltage. The AC/DC hybrid system with an SOP and DNR could address this overvoltage because of the reactive power control from the VSC and SOP. The maximum DG capacity increases to 674 kW (penetration level is approximately 200%), and the highest voltage is approximately 1.05 p.u..

RDG penetration level could not increase at this time because of the capacity limit of VSC3. If this limit is relaxed, the RDG penetration level could increase to approximately 290%.

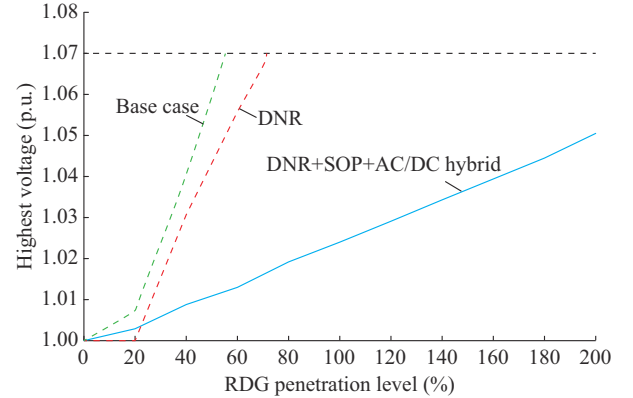


Fig. 9. Highest voltage at different RDG penetration levels.

#### D. Results of Rolling-plan Dispatch Framework

On the basis of the day-ahead input data, random fluctuations of  $\pm 30\%$  and  $\pm 20\%$  [40] are generated for the RDGs and load, respectively, to simulate the intraday 15 min input data at 08:00-10:00, as shown in Fig. 10. The optimized active power of the SOP and VSC for the day-ahead and intraday rolling-plan dispatches are shown in Fig. 11. A positive value indicates that the power flow is in the assumed direction.

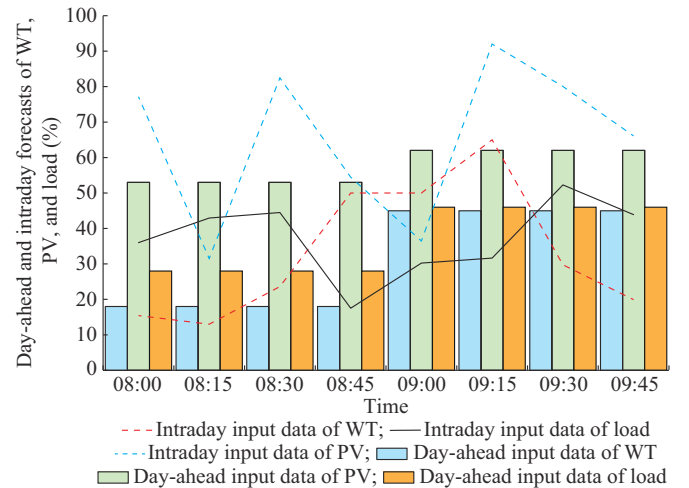


Fig. 10. Intraday 15 min input data of WTs, PVs, and load at 08:00-10:00.

Figure 11 shows that the intraday rolling-plan dispatching result is different from the day-ahead dispatching result at the same time. This is because the active power of the SOP and VSCs changes in real time to adjust to the fluctuations in the WTs, PVs, and load. For example, the output of VSC3 is 205 kW in the rolling-plan dispatch but  $-84.5$  kW in the day-ahead dispatch at 08:15. This is because the intraday input data of the RDGs are 223.17 kW smaller and the load is 113.54 kW larger compared with the day-ahead input data in DC grid 3, thus reversing the entire power demand of DC grid 3. If the rolling-plan dispatch follows the day-

ahead dispatch, load shedding would occur at 08:15. The analyses of VSC3 at 08:45 and 09:15 are the same. Moreover, the output of VSC1 ranges from  $-10$  kW to  $69.27$  kW at 08:45, thus causing the abandonment of RDGs in DC grid 1 because of the increasing output of the RDGs and the decreasing load demand. In summary, if the rolling-plan dispatch follows the dispatching result of the day-ahead dispatch at 08:00-10:00, it causes  $466.42$  kWh of RDG dropout and  $243.40$  kWh of load shedding.

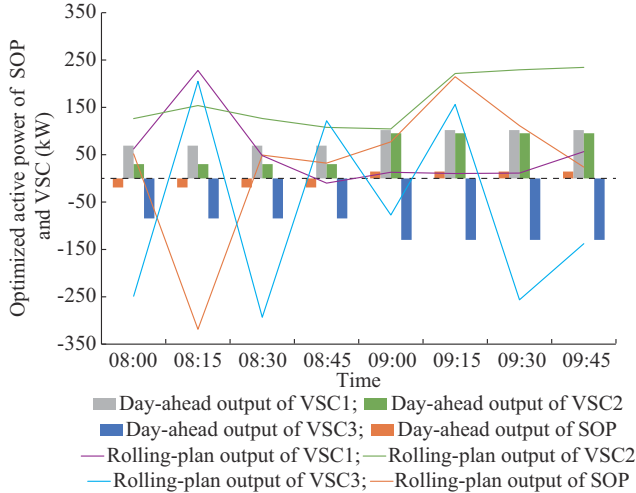


Fig. 11. Optimized active power of SOP and VSC.

To check the switching between the intraday safety dispatch and the economic dispatch of the framework, the RDG penetration level is set to be  $147.8\%$  and  $\tau=0.03$  at 09:15. The voltages at Nodes 25 and 41 are  $0.968$  p.u. and  $1.31$  p.u., respectively, going into the safety dispatch. The node voltages for economic dispatch and safety dispatch at 09:15 are shown in Fig. 12. The voltages at Nodes 25 and 41 are nearly  $1.0$  p.u. less than those in the safety dispatch, and all the node voltages are smoother than those in the economic dispatch. However, the former abandons a  $1.25$  MW of RDG output, whereas none is discarded by the latter.

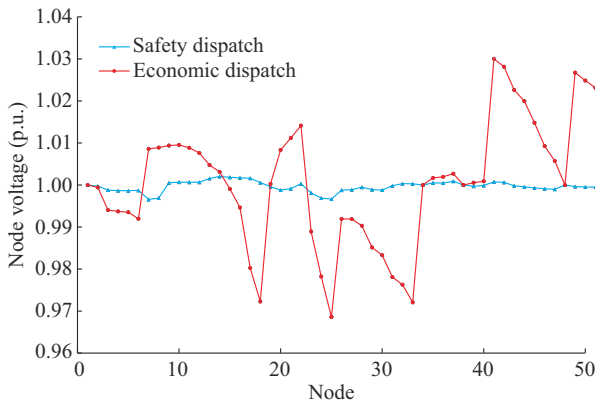


Fig. 12. Node voltages for economic dispatch and safety dispatch at 09:15.

**E. Results of Real-time Feedback Dispatch Framework**

To verify the real-time feedback dispatch, a disturbance within  $\pm 5\%$  and  $\pm 10\%$  is randomly added to the input data of rolling-plan dispatch as the actual data, and the frame-

work is used for dispatching to obtain the power of the tie line, as shown in Fig. 13. From the figure, no matter whether the disturbance is  $\pm 5\%$  or  $\pm 10\%$ , the real-time feedback dispatch of the tie line can follow the power of the rolling-plan dispatch. This result is because the feedback dispatch tracks the power of tie line of the rolling-plan dispatch on the basis of the dispatching of the SOP, VSC, SVC, and RDGs in real time. In addition, the actual data transmitted as feedback to the objective function, i.e., (42), can form a closed loop to prevent error accumulation and increase the effectiveness of the tracking. However, the cost is approximately  $352.42$  kWh of RDG dropout, which is zero in the rolling-plan dispatch. The grid loss exhibits a drop of approximately  $9.3\%$  in the feedback dispatch (from  $84.73$  kWh to  $76.82$  kWh).

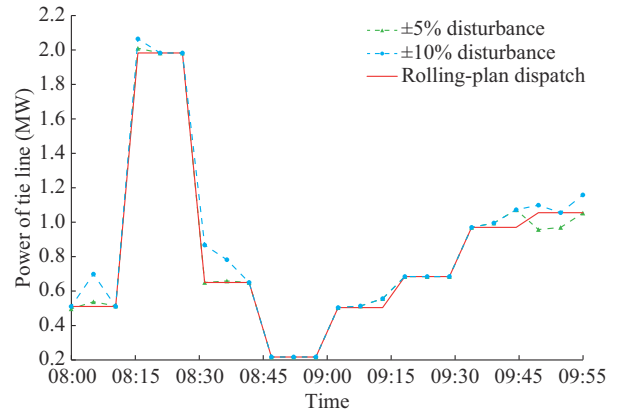


Fig. 13. Power of tie line for disturbances of  $\pm 5\%$  and  $\pm 10\%$  at 08:00-10:00.

Next, the accuracy of the relaxation is confirmed. For day-ahead dispatching, rolling-plan economic dispatch and safety dispatch, the objectives in (29), (40), and (41) are all increasing functions with the current, and their relaxation accuracy has been proven in [41]. Thus, only the relaxation accuracy of (42) is verified. The relaxation gap of the real-time feedback dispatch for a disturbance of  $\pm 10\%$  is shown in Fig. 14. Evidently, the gap is extremely small - the largest is  $8.78 \times 10^{-5}$  at 09:30, which fully meets engineering requirements. Thus, the relaxation method used in this study is satisfactory.

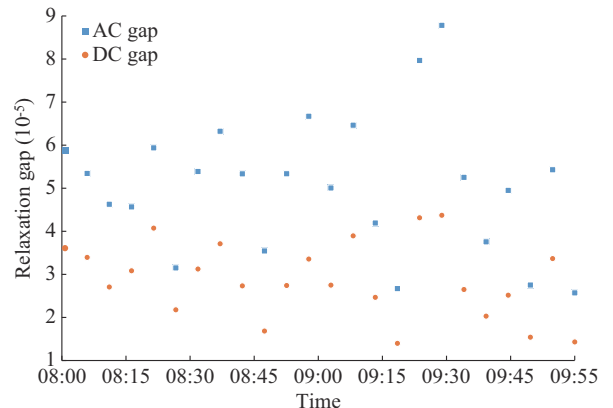


Fig. 14. Relaxation gap of real-time feedback dispatch for a disturbance of  $\pm 10\%$ .

## F. Computational Performance

To test the computational performance of the model and algorithm, test systems 1 (9 nodes), 2 (51 nodes), and 3 (118 nodes) have been utilized. Test systems 1 and 2 have been mentioned in Section V-A; test system 3 uses the modified IEEE 118-node model, whose parameters are given in [42], adding three ESSs, five PVs, and two static var generators (SVGs) at Nodes 16, 39, and 31; Nodes 12, 22, 59, 67, and 113; and Nodes 35 and 97, respectively. The input data are the same as before. The computational information of the test systems in the day-ahead dispatch (Scenario 1), intraday rolling-plan dispatch (Scenario 2), and intraday real-time feedback dispatch (Scenario 3) using the SOCP model are listed in Table VII. The computations have been performed on a personal computer equipped with an AMD Ryzen 5 processor operating at 2.10 GHz and 8 GB of random-access memory (RAM).

TABLE VII  
COMPUTATIONAL INFORMATION OF DIFFERENT TEST SYSTEMS

Test system	Scenario 1		Scenario 2		Scenario 3	
	Time (s)	Max gap ( $10^{-3}$ )	Time (s)	Max gap ( $10^{-3}$ )	Time (s)	Max gap ( $10^{-5}$ )
1	492	5.92	6.03	2.37	3.76	5.38
2	6236	9.78	17.82	8.78	4.23	9.01
3	12537	6.42	22.32	6.04	6.05	4.86

The maximum relaxation gaps of different models in Table VII (“max gap” for short in Table VII) are all extremely small numbers, which fully meet engineering requirements. Essentially, the proposed model is scalable and applicable to large-scale systems (test system 3).

The time of different dispatching scenarios for diverse systems indicates the following. ① As the size of the test system increases, the computation time also increases for each dispatch. ② For the intraday rolling-plan dispatch (Scenario 2) and real-time feedback dispatch (Scenario 3), the computation time is less than 1 min, which is much shorter than the scheduling interval (5 min). ③ For the day-ahead dispatch (Scenario 1), the computation time rapidly increases as the scale of the system increases. This is understandable because day-ahead scheduling creates huge variables for DNR as the test system increases in size. This is also acceptable because the day-ahead dispatch is used to obtain a plan for DNR and the ESSs for the next 24 hours, which means that superior real-time performance is not required.

Additionally, the same experimental conditions and model but with 32 GB of RAM have been used to test the effect of different hardware conditions on the day-ahead dispatch time. The results in three test system reveal that the computation time is reduced by 42.7%, 58.3%, and 71.2%, respectively. Essentially, the time of the day-ahead dispatch could be effectively reduced with an improvement in computer performance. Therefore, with the construction of a big data power platform, the computation time can be considerably reduced as compared to that with a PC. Thus, the proposed method has good engineering applicability.

## VI. CONCLUSION

This study focuses on the uncertainty in a network and established an AC/DC hybrid ADS model considering the DTR, DNR, and SOP. The optimal operation of this ADS is realized through a two-stage scheduling framework of day-ahead and intraday dispatches. The case study shows that the combination of the DTR and AC/DC hybrid system can expand the transmission capacity and alleviate node overvoltage. The synergistic optimization of the SOP and DNR can improve the absorption capacity of RDGs and reduce the line loss. The two-stage optimal dispatching framework can adapt to fluctuations in the RDGs and loads; additionally, it can improve the consumption of RDGs. Intraday feedback dispatching sends the measured data as feedback to track the rolling-plan dispatching plan, thus making the system more suitable for uncertainty.

## REFERENCES

- [1] W. Wang, S. Huang, G. Zhang *et al.*, “Optimal operation of an integrated electricity-heat energy system considering flexible resources dispatch for renewable integration,” *Journal of Modern Power Systems and Clean Energy*, vol. 9, no. 4, pp. 699-710, Jul. 2021.
- [2] S. Su, J. C. Jiang, and W. Wang, “An autonomous decentralized voltage control scheme in PEV charging devices on the distribution network – reactive power compensation for voltage decreases caused by household loads and charging devices,” *International Transactions on Electrical Energy Systems*, vol. 24, no. 3, pp. 412-432, Mar. 2014.
- [3] A. S. A. Awad, D. Turcotte, and T. H. M. El-Fouly, “Impact assessment and mitigation techniques for high penetration levels of renewable energy sources in distribution networks: voltage-control perspective,” *Journal of Modern Power Systems and Clean Energy*, vol. 10, no. 2, pp. 450-458, Mar. 2022.
- [4] X. Shi, R. Qiu, Z. Ling *et al.*, “Spatio-temporal correlation analysis of online monitoring data for anomaly detection and location in distribution networks,” *IEEE Transactions on Smart Grid*, vol. 11, no. 2, pp. 995-1006, Mar. 2020.
- [5] V. Calderaro, G. Conio, V. Galdi *et al.*, “Active management of renewable energy sources for maximizing power production,” *International Journal of Electrical Power & Energy Systems*, vol. 57, pp. 64-72, May 2014.
- [6] Y. Yang, C. Qin, Y. Zheng *et al.*, “Optimal coordinated bidding strategy of wind and solar system with energy storage in day-ahead market,” *Journal of Modern Power Systems and Clean Energy*, vol. 10, no. 1, pp. 192-203, Jan. 2022.
- [7] J. Wu, B. Zhang, L. Hang *et al.*, “Statistical distribution for wind power forecast error and its application to determine optimal size of energy storage system,” *International Journal of Electrical Power & Energy Systems*, vol. 55, pp. 100-107, Feb. 2014.
- [8] D. Liu and K. Sun, “Random forest solar power forecast based on classification optimization,” *Energy*, vol. 187, no. 15, p. 115940, Nov. 2019.
- [9] J. Zhang, J. Yan, D. Infield *et al.*, “Short-term forecasting and uncertainty analysis of wind turbine power based on long short-term memory network and Gaussian mixture model,” *Applied Energy*, vol. 241, pp. 229-244, May 2019.
- [10] Z. Wang, T. Hong, and M. A. Piette, “Building thermal load prediction through shallow machine learning and deep learning,” *Applied Energy*, vol. 263, p. 114683, Apr. 2020.
- [11] A. Lorca and X. A. Sun, “Adaptive robust optimization with dynamic uncertainty sets for multi-period economic dispatch under significant wind,” *IEEE Transactions on Power Systems*, vol. 30, no. 4, pp. 1702-1713, Jul. 2015.
- [12] W. Hou, H. Wei, and R. Zhu, “Data-driven multi-time scale robust scheduling framework of hydrothermal power system considering cascade hydropower station and wind generation,” *IET Generation, Transmission & Distribution*, vol. 13, no. 6, pp. 896-904, Mar. 2019.
- [13] C. Ning and F. You, “A data-driven multistage adaptive robust optimization framework for planning and scheduling under uncertainty,” *AIChE Journal*, vol. 63, no. 10, pp. 4343-4369, May 2017.
- [14] C. Ning and F. You, “Optimization under uncertainty in the era of big

- data and deep learning: when machine learning meets mathematical programming,” *Computers & Chemical Engineering*, vol. 125, no. 9, pp. 434-448, Jun. 2019.
- [15] F. Rodríguez, A. Galarza, J. C. Vasquez *et al.*, “Using deep learning and meteorological parameters to forecast the photovoltaic generators intra-hour output power interval for smart grid control,” *Energy*, vol. 239, p. 122116, Jan. 2022.
- [16] N. Gupta, “Probabilistic optimal reactive power planning with onshore and offshore wind generation, EV and PV uncertainties,” *IEEE Transactions on Industry Applications*, vol. 56, no. 4, pp. 4200-4213, Apr. 2020.
- [17] G. Zhang, J. Yuan, Z. Li *et al.*, “Forming a reliable hybrid microgrid using electric spring coupled with non-sensitive loads and ESS,” *IEEE Transactions on Smart Grid*, vol. 11, no. 4, pp. 2867-2879, Jul. 2020.
- [18] M. Dorostkar-Ghamsari, M. Fotuhi-Firuzabad, M. Lehtonen *et al.*, “Value of distribution network reconfiguration in presence of renewable energy resources,” *IEEE Transactions on Power Systems*, vol. 31, no. 3, pp. 1879-1888, May 2016.
- [19] N. V. Kovacki, P. M. Vidovic, and A. T. Saric, “Scalable algorithm for the dynamic reconfiguration of the distribution network using the Lagrange relaxation approach,” *International Journal of Electrical Power & Energy Systems*, vol. 94, pp. 188-202, Jan. 2018.
- [20] S. Chen, W. Hu, and C. Zhe, “Comprehensive cost minimization in distribution networks using segmented-time feeder reconfiguration and reactive power control of distributed generators,” *IEEE Transactions on Power Systems*, vol. 31, no. 2, pp. 983-993, Mar. 2016.
- [21] D. Kumar, A. Singh, S. K. Mishra *et al.*, “A coordinated planning framework of electric power distribution system: intelligent reconfiguration,” *International Transactions on Electrical Energy Systems*, vol. 28, no. 6, p. 2543, Jun. 2018.
- [22] W. Cao, J. Wu, N. Jenkins *et al.*, “Benefits analysis of soft open points for electrical distribution network operation,” *Applied Energy*, vol. 165, no. 1, pp. 36-47, Mar. 2016.
- [23] L. Peng, H. Ji, C. Wang *et al.*, “Coordinated control method of voltage and reactive power for active distribution networks based on soft open point,” *IEEE Transactions on Sustainable Energy*, vol. 8, no. 4, pp. 1949-3029, Oct. 2017.
- [24] D. Sciano, A. Raza, R. Salcedo *et al.*, “Evaluation of DC links on dense-load urban distribution networks,” *IEEE Transactions on Power Delivery*, vol. 31, no. 3, pp. 1317-1326, Jun. 2016.
- [25] A. Shekhar, L. M. Ramirez-Elizondo, T. B. Soeiro *et al.*, “Boundaries of operation for refurbished parallel AC-DC reconfigurable links in distribution grids,” *IEEE Transactions on Power Delivery*, vol. 35, no. 2, pp. 549-559, May 2019.
- [26] M. Dabbaghjamesh, A. Kavousi-Fard, and S. Mehraeen, “Effective scheduling of reconfigurable microgrids with dynamic thermal line rating,” *IEEE Transactions on Industrial Electronics*, vol. 66, no. 2, pp. 1552-1564, Feb. 2018.
- [27] Y. Li, Y. Wang, and Q. Chen, “Optimal dispatch with transformer dynamic thermal rating in ADNs incorporating high PV penetration,” *IEEE Transactions on Smart Grid*, vol. 12, no. 3, pp. 1989-1999, May 2021.
- [28] H. M. A. Ahmed and M. M. A. Salama, “Energy management of AC-DC hybrid distribution systems considering network reconfiguration,” *IEEE Transactions on Power Systems*, vol. 34, no. 6, pp. 4583-4594, Nov. 2019.
- [29] Y. Fu, Z. Zhang, Z. Li *et al.*, “Energy management for hybrid AC/DC distribution system with microgrid clusters using non-cooperative game theory and robust optimization,” *IEEE Transactions on Smart Grid*, vol. 11, no. 2, pp. 1510-1525, Mar. 2020.
- [30] C. Qi, K. Wang, Y. Fu *et al.*, “A decentralized optimal operation of AC/DC hybrid distribution grids,” *IEEE Transactions on Smart Grid*, vol. 9, no. 6, pp. 6095-6105, Nov. 2018.
- [31] A. Azizivahed, A. Arefi, S. Ghavidel *et al.*, “Energy management strategy in dynamic distribution network reconfiguration considering renewable energy resources and storage,” *IEEE Transactions on Sustainable Energy*, vol. 11, no. 2, pp. 662-673, Apr. 2020.
- [32] H. Ji, P. Li, J. Ji *et al.*, “MPC-based local voltage control strategy of DGs in active distribution networks,” *IEEE Transactions on Sustainable Energy*, vol. 11, no. 4, pp. 2911-2921, Oct. 2021.
- [33] W. Jiao, J. Chen, Q. Wu *et al.*, “Distributed coordinated voltage control for distribution networks with DG and OLTC based on MPC and gradient projection,” *IEEE Transactions on Power Systems*, vol. 37, no. 1, pp. 680-690, Jan. 2022.
- [34] X. Liu, “Multiple time-scale economic dispatching strategy for commercial building with virtual energy storage under demand response mechanism,” *International Journal of Energy Research*, vol. 45, no. 6, pp. 16204-16227, May 2021.
- [35] A. A. Eajal, M. F. Shaaban, K. Ponnambalam *et al.*, “Stochastic centralized dispatch scheme for AC/DC hybrid smart distribution systems,” *IEEE Transactions on Sustainable Energy*, vol. 7, no. 3, pp. 1046-1059, Jul. 2017.
- [36] M. Isuru, M. Hotz, H. B. Gooi *et al.*, “Network-constrained thermal unit commitment for hybrid AC/DC transmission grids under wind power uncertainty,” *Applied Energy*, vol. 258, p. 114031, Jan. 2020.
- [37] L. Zhang, J. Liang, W. Tang *et al.*, “Converting AC distribution lines to DC to increase transfer capacities and DG penetration,” *IEEE Transactions on Smart Grid*, vol. 10, no. 2, pp. 1477-1487, Mar. 2019.
- [38] Y. Wang, D. Liu, X. Xu *et al.*, “Cyber-physical power system modeling for timing-driven control of active distribution network,” *Journal of Modern Power Systems and Clean Energy*, vol. 8, no. 3, pp. 549-556, May 2020.
- [39] W. D. Fisher, “On grouping for maximum homogeneity,” *Journal of the American Statistical Association*, vol. 53, no. 284, pp. 789-798, Jan. 1958.
- [40] A. Costa, A. Crespo, J. Navarro *et al.*, “A review on the young history of the wind power short-term prediction,” *Renewable and Sustainable Energy Reviews*, vol. 12, no. 6, pp. 1725-1744, Aug. 2008.
- [41] L. Gan, N. Li, U. Topcu *et al.*, “Exact convex relaxation of optimal power flow in radial networks,” *IEEE Transactions on Automatic Control*, vol. 60, no. 1, pp. 72-87, Jan. 2015.
- [42] T. Yuan, K. Wang, G. Li *et al.*, “Affinely adjustable robust AC-DC optimal power flow considering correlation of wind power,” *IET Renewable Power Generation*, vol. 12, no. 13, pp. 1478-1485, May 2018.

**Yi Su** received his B.S. degree in electrical engineering and automation from Wuhan University of Technology, Wuhan, China, in 2009, and his M. S. degree in electrical engineering from Hunan University, Changsha, China, in 2016. He is currently pursuing a Ph.D. degree in power systems and energy conversion at Universiti Sains Malaysia (USM), Penang, Malaysia. From 2016 to 2020, he was an Engineer at China Southern Power Grid, Guangzhou, China. His research interests include resilience of distribution networks, optimized control of power systems, and intelligent information processing.

**Jiashen Teh** received his B.Eng. degree (Hons.) in electrical and electronic engineering from Universiti Tenaga Nasional, Penang, Malaysia, in 2010, and his Ph.D. degree in electrical and electronic engineering from The University of Manchester, Manchester, U.K., in 2016. Since 2016, he has been a Senior Lecturer/Assistant Professor at Universiti Sains Malaysia (USM), Penang, Malaysia. In 2018, he was appointed and served as an Adjunct Professor for the Green Energy Electronic Center, National Taipei University of Technology (Taipei Tech), Taipei, China. Since 2019, he has been an Adjunct Professor at the Intelligent Electric Vehicle and Green Energy Center, National Chung Hsing University, Taichung, China. He is a Chartered Engineer conferred by the Engineering Council, U.K. and The Institution of Engineering and Technology, as well as a registered Professional Engineer with the Board of Engineers Malaysia. He is a member of the IEEE Power and Energy Society and the Institution of Engineers, Malaysia. His research interests include probabilistic modeling of power systems, grid integration of renewable energy resources, and reliability modeling of smart grid.